

Application of Statistical Cancer Atlas for 3D Biopsy

Ramkrishnan Narayanan^a, Dinggang Shen^b, Christos Davatzikos^b, E David Crawford^c,
Albaha Barqawi^c, Priya Werahera^c, Dinesh Kumar^a and Jasjit S Suri^a

^aEigen LLC, 13366 Grass Valley Ave., Grass Valley, CA 95945

^bSec. of Biomedical Image Analysis, Dept. of Radiology, Univ. of Pennsylvania, PA 19104

^c University of Colorado Hospital, Denver, CO 80262

ABSTRACT

Prostate cancer is the most commonly diagnosed cancer in males in the United States and the second leading cause of cancer death. While the exact cause is still under investigation, researchers agree on certain risk factors like age, family history, dietary habits, lifestyle and race. It is also widely accepted that cancer distribution within the prostate is inhomogeneous, i.e. certain regions have a higher likelihood of developing cancer. In this regard extensive work has been done to study the distribution of cancer in order to perform biopsy more effectively. Recently a statistical cancer atlas of the prostate was demonstrated along with an optimal biopsy scheme achieving a high detection rate.

In this paper we discuss the complete construction and application of such an atlas that can be used in a clinical setting to effectively target high cancer zones during biopsy. The method consists of integrating intensity statistics in the form of cancer probabilities at every voxel in the image with shape statistics of the prostate in order to quickly warp the atlas onto a subject ultrasound image. While the atlas surface can be registered to a pre-segmented subject prostate surface or instead used to perform segmentation of the capsule via optimization of shape parameters to segment the subject image, the strength of our approach lies in the fast mapping of cancer statistics onto the subject using shape statistics. The shape model was trained from over 38 expert segmented prostate surfaces and the atlas registration accuracy was found to be high suggesting the use of this method to perform biopsy in near real time situations with some optimization.

Keywords: prostate, registration, atlas, shape, cancer

1. INTRODUCTION

The Center for Prostate Disease Research (CPDR) estimates that prostate cancer accounts for nearly 30% of cancers affecting males in the United States and over 27,000 deaths in 2007. Although prostate cancers grow slowly the risk of metastasis increases over time. If diagnosed early, the cancer can be confined to the prostate and the survival rate after treatment approaches 100%. Prostate specific antigen (PSA) measured through a blood test and the digital rectal examination (DRE) are among the most commonly used methods to screen for prostate cancer. Although radical prostatectomy is an option when the cancer is localized to the prostate, several less invasive procedures like transrectal ultrasound (TRUS) guided biopsy is known to cause less morbidity, faster recovery time and reduced costs, and is now a standard method.¹ Contrast-enhanced ultrasound imaging techniques using microbubble contrast agents² may be able to detect cancer lesions that may be normally invisible by conventional grayscale imaging and is an area of active interest.

The protocols concerning biopsy widely vary and several modifications to the popular sextant biopsy³ have been reported. Authors in⁴ added two additional median cores on both sides to compare a ten core biopsy with their modified sextant biopsy reporting 32% and 40% for six and ten cores respectively. Over the years the number of cores have increased to over fifteen leading to minor complications such as rectal bleeding, hematuria and hematospermia without significant improvement in detection rates. In a study, Naughton et al⁵ report that only increasing the number of cores from six to twelve did not lead to any improvement. Chen et al⁶ report an 11-core multi-site biopsy including 1 sextant, 1 posterior midline, 2 transition and 2 anterior horn cores

Further author information: (Send correspondence to R. Narayanan)

R. Narayanan: E-mail: ram.narayanan@eigen.com, Telephone: 1 530 274 1240 Extn: 210

Image Processing: Algorithms and Systems VI, edited by Jaakko T. Astola,
Karen O. Egiazarian, Edward R. Dougherty, Proc. of SPIE-IS&T Electronic Imaging,
SPIE Vol. 6812, 681216, © 2008 SPIE-IS&T · 0277-786X/08/\$18

SPIE-IS&T Vol. 6812 681216-1

improving detection rates to 85% and 70% in prostates less than 50g and greater than 50g respectively. This study strongly suggests that the location is a very strong determining factor in significantly improving detection rates and cannot be directly linked to the number of cores chosen. A 3D prostate model was developed in⁷ showing the distribution of cancers among various zones. In Opell et al⁸, authors develop a spatial distribution map of cancers in the prostate concluding that the cancers are more commonly found in the posterior half, apical and mid regions of the prostate and suggesting its use to develop more sophisticated biopsy protocols. Shen et al⁹ developed a statistical cancer atlas of the prostate from over 100 subjects from the CPDR database. In addition to developing a voxel based probabilistic map, the authors also developed an optimal biopsy strategy to maximize the probability of detecting cancer. They showed a significantly improved detection rate of almost 100% using only seven needles under needle placement uncertainties. In a more recent development¹⁰, the method in⁹ was further improved upon by modeling the shape of the needle, dividing the subject database into groups based on race, age and PSA level, and an automatic segmentation strategy to segment the capsule from the acquired ultrasound image.

In our work in this paper, we use many of the tools and data already developed by the authors in^{9,10} and demonstrate the fast registration of such an atlas to patients undergoing biopsy. The optimal needle locations and a 3D cancer probability map are registered to the subject using shape statistics of the prostate learned from a large population of expert segmented images after removing global rotational, scale and translation variations across the subjects. The shape statistics are in the form of a mean surface, principal component analysis (PCA) basis shapes and their Eigenvalues. The cancer atlas is integrated with the mean surface through registration of the mean surface and the atlas surface resulting in the atlas volume being completely defined within the mean surface. Any warping applied to the mean surface is consequently applied to the atlas volume to drive it into registration with the subject's U/S image.

In our experiments, the subject ultrasound images were segmented to distinguish the capsule from data outside it. The mean surface was driven in to registration to this segmented surface via a fast registration method using shape statistics. The correspondences obtained through this registration were then used to warp the atlas volume to the subject image. The registration accuracy measured as intersection-union ratio (IUR)¹¹ in all our simulations were typically above 0.8 using shape priors. We show that our model based registration method can be used to accurately and quickly warp the atlas volume to the subject in a clinical setting after some optimization. The detection accuracy of the atlas and its performance are the same as shown in¹⁰ with over 90% detection accuracy using very few needles.

2. DATA PREPARATION

There are two offline steps involved in the construction of the atlas and warping it to patient data

1. The collection of cancer labels from a large population of prostatectomy specimen to build the intensity statistics at voxel locations in the 3D model of the prostate.
2. Training of the prostate shape model from several expert segmented surfaces to learn the possible modes of variation of the prostate in order to efficiently warp it on to the subject ultrasound image during biopsy.

The first step was already completed by our collaborators who have previously demonstrated the construction of a 3D atlas.^{9,10} They were able to show that a cancer detection rate of 94-96% could be achieved using only 6-7 biopsy cores. We have briefly outlined the steps they followed in order to construct such an atlas. They have also shown the alignment of such an atlas with the patient data via surface registration of the patient's segmented prostate using¹² followed by elastic warping¹³ to interpolate the boundary conditions to the entire atlas volume. These methods although robust, may be impractical in a real setting where the registration of the atlas must be fast in addition to being accurate. We will discuss our method where we used shape priors to help improve the speed of our algorithm. We will also discuss other optimizations possible within the scope of our future work.

2.1 Cancer Data Description

The cancer data for the atlas was a result of the work done by the authors in^{9,10}. The following is a brief summary of their effort. 64 prostatectomy specimens from the CPDR tissue bank were used in the preparation of the atlas. They were whole mounted and step-sliced at 2.25 mm. 5 μm thick sections were then stained with haematoxylin and eosin. These specimens were pathologically reviewed for tumors by an expert, reconstructed in 3D and labeled based on cancers and normal tissue. The absence of anatomical information precluded registration of the atlas directly in 3D. Instead the surfaces for each of the images were extracted and registered using Adaptive Focus Deformation Model (AFDM) described in¹² followed by elastic warping.

2.2 Prostate Shape Model Construction

In order to compute the modes of variation of the prostate surface, a shape model of the prostate must be constructed. A shape model is supplied with corresponding labels or "landmark" points throughout the surface of the prostate. These landmarks define the shape of an individual prostate and also identify corresponding regions of anatomical similarity across the training set. The training begins with the collection of training data which in our case is a set of expert segmented prostate surfaces. One of the surfaces in the set is picked as the model and all the other surfaces are registered to it. The output of the registration algorithm is a set of deformed surfaces for each of the target surfaces in the training set. The set of vertices in the model and each of the deformed surfaces define a correspondence. We used the AFDM to register 38 expert segmented surfaces to a previously chosen model surface from one of the 38 surfaces. The registration accuracy was measured based on the surface overlap of the deformed model surface after registration and the respective target using IUR. The average IUR after 37 registrations was found to be 0.9848 for an average starting IUR of 0.5267.

Once labeled, shape model construction begins with the removal of global rotation, translation and scale parameters thus removing global variability in order to model purely morphological shape change. The method followed is as described in Cootes¹⁴ to create a set of aligned surfaces $D = (\mathbf{x}_1 \mathbf{x}_2 \cdots \mathbf{x}_N)$ where \mathbf{x}_i is a vector containing all vertices describing the i th surface, and the mean surface after removing global variations. The Eigenvalues and Eigenvectors spanning the set of shapes in D are computed. In our experiment we found that the Eigenvectors corresponding to the 15 largest Eigenvalues accounted for more than 95% variation in the data and only these Eigenvectors were used in our shape based registration strategy described in a later section. The result of the shape model construction is the set of all possible shapes that span the space of D , i.e. $\mathbf{y} = \bar{\mathbf{x}} + \sum_{i=1}^{15} \alpha_i \mathbf{v}_i$ where $\bar{\mathbf{x}}$ is the mean shape, \mathbf{v}_i is the i th Eigenvector and α_i is the set of projections on each Eigenvector.

2.3 Shape-Cancer Statistics Integration

In order to use the shape priors to warp the atlas surface to the segmented subject, the shape priors must be integrated with the atlas, i.e. the atlas surface must correspond with the mean surface. This is achieved by registering the atlas surface with the mean surface. The correspondence obtained is then used to elastically interpolate the entire atlas volume so that it now resides within the mean surface. Any warping applied to the mean surface can now be interpolated to warp the entire atlas volume. Fig. 1 shows the original mean shape and atlas surface in the top row. The atlas is deformed to register with the mean surface shown in the bottom row (right) and finally the entire atlas volume is elastically deformed to warp to the mean surface shown at the bottom right.

3. WARPING ATLAS TO SUBJECT

The atlas is now completely defined in the mean surface which can be deformed using model priors to generate any shape within the span of all shapes defined by the Eigenvectors. This way, the mean surface can be warped through the optimization of shape parameters to perform segmentation directly on the 3D patient ultrasound volume or registered on to a previously segmented subject surface. In both cases model priors are used to deform the mean shape to the prostate capsule of the subject.

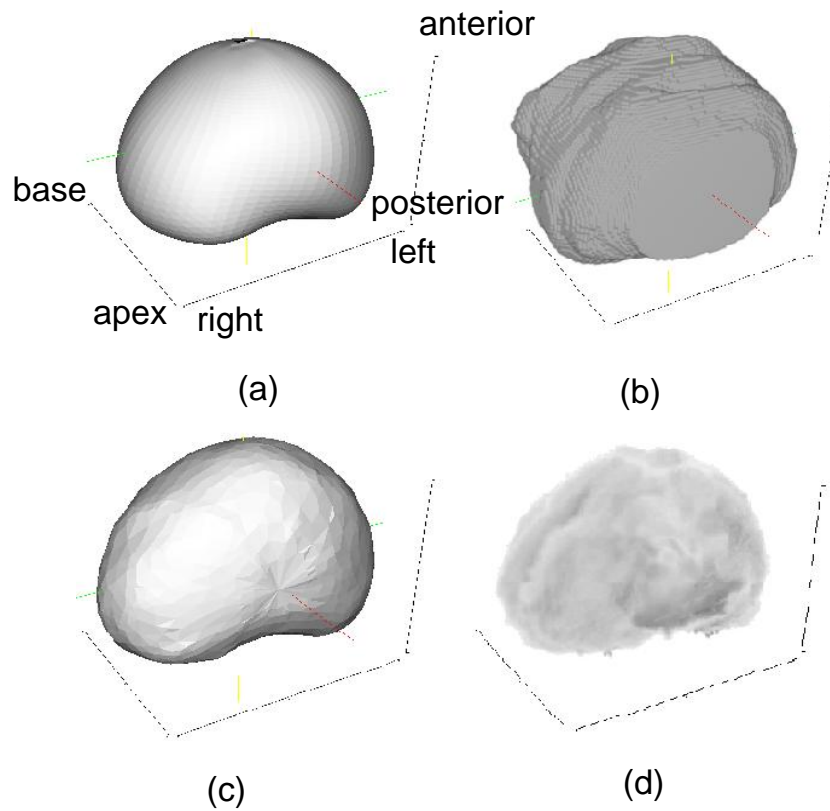


Figure 1. Top left image is the mean surface iteratively found from the aligned shapes. Top right image is the atlas surface after normalizing all prostatectomy samples that were reconstructed to 3D. Bottom left image shows the surface after warping the atlas surface to the mean surface. The bottom right image shows the 3D probability map after elastically warping the entire atlas volume using the surface boundary conditions to lie within the mean surface. Darker regions show regions with higher probability.

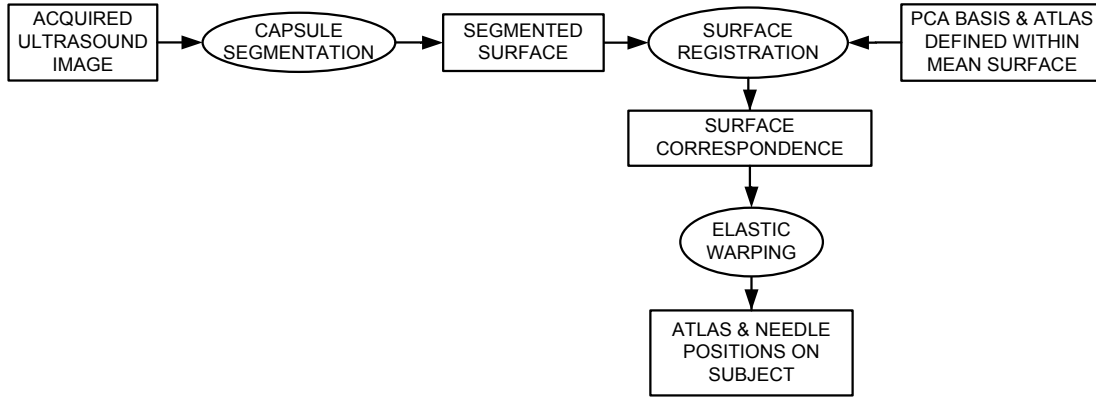


Figure 2. Flowchart of the system that warps the atlas to subject.

3.1 Prostate Segmentation

In our experiments we warped our mean surface to a previously segmented prostate volume using the method outlined in.¹⁵ In this method the authors used a discrete dynamic contour (DDC) to segment capsule boundaries based on edge gradients, contour smoothness and a damping force related to the contour velocity. The segmentation was performed on a 2D plane that was rotated about the anterior-posterior axis at the center of the image containing the prostate. The segmentation was performed on each plane one at a time before obtaining a new plane view spaced at an angle of 3 degrees about the axis. Segmentation of the 3D capsule took about 8 seconds on a 3.2 GHz Pentium 4 with 3 Gb memory.

3.2 Atlas Warping

Due to the absence of any anatomic information in the atlas only surface information is used for registering it with the segmented prostate capsule of the subject. This is achieved by first registering the mean surface with the subject's segmented capsule using the shape model. The correspondences obtained throughout the surface are used as boundary conditions to solve the partial differential equations governing an elastic material. The solution to this PDE provides the warp at every voxel in the atlas. Fig. 2 shows the flowchart of the system.

The mean surface ($\bar{\mathbf{x}}$) can be registered on to the subject's prostate surface (\mathbf{y}) in two ways. The first method -data driven registration (DD) follows Shen's method¹⁶ where the deformation is directly applied to the mean surface vertices to best find the best deformation that minimizes cost. This is estimated by deforming the mean vertices in the direction of the nearest subject vertex. Let the matrix of Eigenvectors be $H = [\mathbf{v}_1 \mathbf{v}_2 \dots \mathbf{v}_N]$. The model based warps are computed through the following steps:

1. Set model based warp: $\mathbf{x}_{model} = \bar{\mathbf{x}}$.
2. $\mathbf{x}_{model} \rightarrow \mathbf{x}' (= \mathbf{x}_{model} + d)$ where d is the vertex displacement vector so as to minimize $\|\mathbf{x}' - \mathbf{y}\|$.
3. Estimate Procrustes parameters: $(\hat{\mathbf{t}}, \hat{R}, \hat{c}) = \underset{(\mathbf{t}, R, c)}{\operatorname{argmin}} \|\bar{\mathbf{x}} - \mathbf{x}''\|$, where $\mathbf{x}'' = cR\mathbf{x}' + \mathbf{t}$ and \mathbf{t} , R and c are the global translation, rotation and scale parameters.
4. Estimate model based warp: $\mathbf{x}_{model} = HH^T(\mathbf{x}'' - \bar{\mathbf{x}}) + \bar{\mathbf{x}}$.
5. Repeat steps 2 to 4 until $\|\mathbf{x}' - \mathbf{y}\|$ is minimized in 2.

This method results in very small registration errors if the surfaces resemble the training set. However due to the deformations at every vertex calculated in step 1, it may be slow. Optionally the surface can be sub-sampled where not all vertices are warped and the approximation might be tolerable. The second method of surface registration - model driven (MD) approach is where the shape parameters are explicitly optimized where only warps permitted by the shape model are directly optimized. Here the projections on the Eigenvectors (α) and the global rotation, scale and translation parameters are estimated as

$$(\hat{\alpha}, \hat{\mathbf{t}}, \hat{R}, \hat{c}) = \arg \min_{(\alpha, \mathbf{t}, R, c)} \|cR(H\alpha + \bar{\mathbf{x}}) + \mathbf{t} - \mathbf{y}\| \quad (1)$$

The gradients and the Hessian are estimated through stochastic approximation (SA) via “simultaneous perturbation” of parameters discussed in.¹⁷ Using this method only four function evaluations are needed to compute the gradient and Hessian at each iteration. Using one-sided randomized differences,¹⁸ Hessian and gradient approximations can be computed using three function evaluations and the solution found using Levenberg-Marquardt¹⁹ optimization. The correspondences obtained using either the model driven or the data driven approach are used to interpolate the entire volume using an elastic deformation model described in.¹³

4. RESULTS

Table 1. Shows the original segmented subject volume and the estimated warped mean volume using both data and model driven methods. The mean volume before warping was 41.7 cc. Column 5 shows the original IUR followed by the final IUR from both methods

#	Orig. Sub.	Est. Vol. (cc)		Orig. IUR	Final IUR	
	Vol. (cc)	Model	Data		Model	Data
1	37.4	36.1	36.5	0.563	0.802	0.891
2	69.2	66.7	67.4	0.548	0.873	0.902
3	42.7	45.2	42.3	0.414	0.805	0.846
4	52.7	49.8	51.6	0.384	0.882	0.917
5	24.8	24.3	23.7	0.267	0.788	0.845
6	29.2	27.5	28.1	0.244	0.763	0.880
7	73.3	69.7	72.6	0.445	0.811	0.880
8	19.2	19.3	20.0	0.160	0.813	0.894
9	29.5	28.9	29.2	0.262	0.826	0.895
10	89.8	92.3	89.5	0.463	0.898	0.901
11	69.1	71.6	69.4	0.434	0.798	0.869
12	44.7	43.9	44.3	0.385	0.850	0.877
13	36.3	37.0	36.2	0.464	0.842	0.876
14	17.5	18.4	17.7	0.242	0.641	0.846
15	32.0	32.5	32.0	0.223	0.858	0.885
16	26.1	24.5	24.6	0.217	0.772	0.844
17	17.6	19.9	17.7	0.251	0.595	0.800
18	26.7	25.7	26.0	0.283	0.814	0.895
19	41.4	40.7	40.5	0.315	0.845	0.889
20	40.1	39.4	40.2	0.301	0.817	0.884
			Mean IUR	0.343	0.805	0.876

The performance of the two methods were compared. The mean surface was registered on to twenty previously segmented volumes using both strategies - data and model driven. The registration accuracy was measured as the ratio of intersection to union of the two surfaces, i.e. the warped mean and each of the computer segmented capsules. The known subject capsule volume and the estimated capsule volume from both methods were also compared. Table 1 shows volume estimates and IUR from both methods. The original volume enclosed within the mean surface was 41.7 cc. Since the mean surface is registered on to a previously segmented surface, segmentation errors are likely to result in shapes that may lie outside the span of the shape model. As a result the estimates for IUR are probably conservative. The average IUR after 50 gradient steps for 15 parameter optimization was found to be 0.8052 and the average for the data driven method was 0.8763. Fig. 3(a) shows the mean surface and the segmented subject capsule before registration. (b) shows the result of surface registration after warping the mean surface to the capsule. (c) shows the complete atlas volume warped from mean shape in (a) to the subject capsule. Finally (d) shows the optimal needle biopsy locations on the subject capsule pre-computed from the atlas so as to maximize probability of cancer detection.

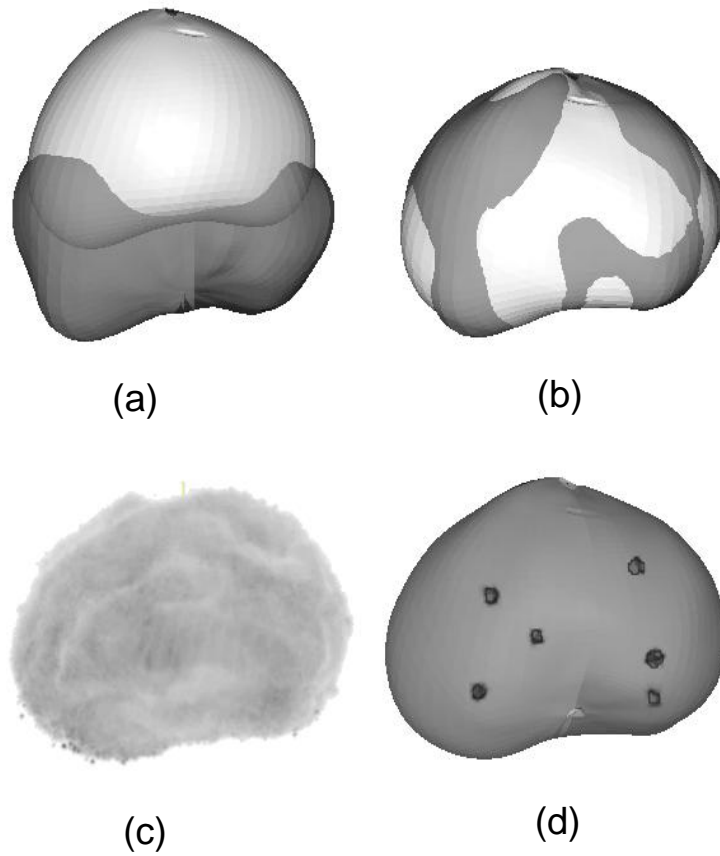


Figure 3. (a) Mean surface on top and subject capsule in grey below. (b) Warped mean surface subject capsule after surface registration. (c) Atlas warped to subject using surface correspondence. (d) Optimal needle positions on subject capsule.

5. DISCUSSION

Both methods ran in under 30 seconds. Further optimization is possible by reducing the number of vertices (now using 4000) or using fewer vertex points in calculating cost. A combination of the two methods is also possible using the model driven optimization of the first 4-8 projections corresponding to the largest Eigenvalues (coarsely warping) followed by the data driven approach to fine tune the parameters. The surface registration was followed by elastic warping to find the warp inside the mean surface (atlas) to register it to the subject. It should be noted that warping the entire volume of the atlas is not necessary if only the new needle locations in Fig. 3(d) are to be computed. This saves several seconds during biopsy resulting in following steps - capsule segmentation followed by surface registration and interpolation to find new needle locations.

6. CONCLUSION

In this paper we discussed two methods to obtain surface correspondence between the atlas and the segmented capsule. Both methods ran in less than 30 seconds in MATLAB (Pentium 4, 3 GHz with 3 Gb) potentially leading to further improvement in compute time running in C with some optimization suggesting its applicability in a clinical setting during biopsy. The volume elastic warping routine running 500 iterations ran in under 30 seconds in C. Fewer iterations may be enough to achieve sufficiently high accuracy. Further a 3D shape model could be simultaneously trained using the elastic warping PDE solution for the entire training data simultaneously with the surfaces. The fast surface registration correspondences may then be used as predictors for the entire 3D deformation field similar to the method used in.²⁰ The volume warping (via elastic or a 3D shape model) can be completely avoided if only optimal needle locations were being computed. Future work would also involve studying the sensitivity of biopsy needle locations to surface registration accuracy, i.e. lower sensitivity of needle locations to surface registration would be preferred.

REFERENCES

1. B. Djavan, M. Remzi, K. Ghawidel, and K. Marberger, "Diagnosis of prostate cancer: The clinical use of transrectal ultrasound and biopsy," *EAU* **1**, pp. 9–15, 2003.
2. E. J. Halpern, "Contrast-enhanced ultrasound imaging of prostate cancer," *Reviews in Urology* **8**(1), pp. S29–S37, 2006.
3. K. K. Hodge, J. E. McNeal, M. Terris, and T. A. Stamey, "Random systematic versus directed ultrasound-guided transrectal core biopsies of the prostate," *J Urol*, 1989.
4. R. Paul, S. Scholer, H. van Randerborgh, H. Kubler, M. Alschibaja, R. Busch, and R. Hartung, "Optimization of prostatic biopsy: A prospective randomized trial comparing the sextant biopsy with a 10-core biopsy impact of prostatic region of sampling," *Urol Int* **74**, pp. 203–208.
5. C. K. Naughton, D. C. Miller, D. E. Mager, D. K. Ornstein, and W. J. Catalona, "A prospective randomized trial comparing 6 versus 12 prostate biopsy cores: impact on cancer detection," *J Urol*. **164**, pp. 388–392.
6. M. E. Chen, P. Troncoso, K. Tang, R. J. Babaian, and D. Johnston, "Comparison of prostate biopsy schemes by computer simulation," *J Urol*. **53**, pp. 951–960.
7. M. B. Opell, J. Zeng, J. J. Bauer, R. R. Connelly, W. Zhang, I. A. Sesterhenn, S. K. Mun, J. W. Moul, and J. H. Lynch, "Modeling and mapping of prostate cancer," *Computers and Graphics* **24**, pp. 683–694, 2000.
8. M. B. Opell, J. Zeng, J. J. Bauer, R. R. Connelly, W. Zhang, I. A. Sesterhenn, S. K. Mun, J. W. Moul, and J. H. Lynch, "Investigating the distribution of prostate cancer using three-dimensional computer simulation," *Prostate Cancer and Prostatic Diseases* **5**, pp. 204–208, 2002.
9. D. Shen, Z. Lao, J. Zeng, W. Zhang, I. A. Sesterhenn, L. Sun, J. W. Moul, E. H. Herskovits, G. Fichtinger, and C. Davatzikos, "Optimized prostate biopsy via a statistical atlas of cancer spatial distribution," *Medical Image Analysis* **8**, pp. 139–150, 2004.
10. Y. Zhan, D. Shen, J. Zeng, L. Sun, G. Fichtinger, J. Moul, and C. Davatzikos, "Targeted prostate biopsy using statistical image analysis," *IEEE Trans. Med. Imag.* **26**(6), pp. 779–788, 2007.
11. R. Dann, J. Holford, S. Kovacic, M. Reivich, and R. Bajcsy, "Evaluation of elastic matching for anatomic (ct,mr) and functional (pet) cerebral images," *J. Comput. Assist. Tomography* **13**, pp. 603–611, 1989.

12. D. G. Shen, E. Herskovits, and C. Davatzikos, "An adaptive focus statistical shape model for segmentation and shape modeling of 3D brain structures," *IEEE Trans. Med. Imag.* **20**, pp. 257–271, 2001.
13. C. Davatzikos, "Spatial transformation and registration of brain images using elastically deformable models," *Comp. Vision and Image Understanding* **66**(2), pp. 207–222, 1997.
14. T. F. Cootes, C. J. Taylor, D. H. Cooper, and J. Graham, "Active shape models - their training and application," *Computer Vision and Image Understanding* **61**(1), pp. 38–59, 1995.
15. H. M. Ladak, F. Mao, Y. Wang, D. B. Downey, D. A. Steinman, and A. Fenster, "Prostate boundary segmentation from 2d ultrasound images," *Engg. in Medicine and Biology Society, Proc of the 22nd Annual Int. Conf. of IEEE* **4**, pp. 3188–3191, 2000.
16. D. Shen and C. Davatzikos, "An adaptive-focus deformable model using statistical and geometric information," *IEEE Trans. on Pattern Anal. and Machine Intelligence* **22**(7), pp. 1–8, 2000.
17. J. C. Spall, "Adaptive stochastic approximation by the simultaneous perturbation method," *IEEE Trans. on Automatic Control* **45**(10), pp. 1839–1853, 2000.
18. H. F. Chen, T. E. Duncan, and B. Pasik-Duncan, "A stochastic approximation algorithm with random differences," *13th Triennial World Congress*, pp. 493–496, 1996.
19. D. W. Marquardt, "An algorithm for least-squares estimation of non-linear parameters," *J. Soc. Ind. Appl. Math.* **11**, pp. 431–441, 1963.
20. C. Davatzikos, D. Shen, A. Mohamed, and S. K. Kyriacou, "A framework for predictive modeling of anatomical deformations," *IEEE Trans. Med. Imag.* **20**, pp. 836–843, 2001.